PROCEEDINGS OF SPIE

Optics and Photonics for Information Processing X

Khan M. Iftekharuddin
Abdul A. S. Awwal
Mireya García Vázquez
Andrés Márquez
Mohammad A. Matin
Editors

29–30 August 2016
San Diego, California, United States

Sponsored and Published by
SPIE

Volume 9970

Proceedings of SPIE 0277-786X, V. 9970

SPIE is an international society advancing an interdisciplinary approach to the science and application of light.

Optics and Photonics for Information Processing X, edited by Khan M. Iftekharuddin, Abdul A. S. Awwal, Mireya García Vázquez, Andrés Márquez, Mohammad A. Matin, Proc. of SPIE Vol. 9970, 997001 · © 2016 SPIE · CCC code: 0277-786X/16/$18 · doi: 10.1117/12.2256424

The papers in this volume were part of the technical conference cited on the cover and title page. Papers were selected and subject to review by the editors and conference program committee. Some conference presentations may not be available for publication. Additional papers and presentation recordings may be available online in the SPIE Digital Library at SPIEDigitalLibrary.org.

The papers reflect the work and thoughts of the authors and are published herein as submitted. The publisher is not responsible for the validity of the information or for any outcomes resulting from reliance thereon.

Please use the following format to cite material from these Proceedings:
Author(s), "Title of Paper," in *Optics and Photonics for Information Processing X*, edited by Khan M. Iftekharuddin, Abdul A. S. Awwal, Mireya García Vázquez, Andrés Márquez, Mohammad A. Matin, Proceedings of SPIE Vol. 9970 (SPIE, Bellingham, WA, 2016) Six-digit Article CID Number.

ISSN: 0277-786X
ISSN: 1996-756X (electronic)
ISBN: 9781510603318
ISBN: 9781510603325 (electronic)

Published by
SPIE
P.O. Box 10, Bellingham, Washington 98227-0010 USA
Telephone +1 360 676 3290 (Pacific Time) · Fax +1 360 647 1445
SPIE.org

Printed in the United States of America.

Publication of record for individual papers is online in the SPIE Digital Library.

SPIE. DIGITAL LIBRARY
SPIEDigitalLibrary.org

Paper Numbering: *Proceedings of SPIE* follow an e-First publication model. A unique citation identifier (CID) number is assigned to each article at the time of publication. Utilization of CIDs allows articles to be fully citable as soon as they are published online, and connects the same identifier to all online and print versions of the publication. SPIE uses a six-digit CID article numbering system structured as follows:

- The first four digits correspond to the SPIE volume number.
- The last two digits indicate publication order within the volume using a Base 36 numbering system employing both numerals and letters. These two-number sets start with 00, 01, 02, 03, 04, 05, 06, 07, 08, 09, 0A, 0B … 0Z, followed by 10-1Z, 20-2Z, etc. The CID Number appears on each page of the manuscript.

Contents

PVA/AA photopolymers and PA-LCoS devices combined for holographic data storage

Andrés Márquez[1,2], Francisco J. Martínez[1,2], Roberto Fernández[1,2], Sergi Gallego[1,2], Mariela L. Álvarez[1,2], Inmaculada Pascual[2,3], Augusto Beléndez[1,2]

[1]Dept. de Física, Ing. de Sistemas y T. Señal, Univ. de Alicante, Ap. 99, E-03080, Alicante, Spain
[2]I.U. Física Aplicada a las Ciencias y las Tecnologías U. de Alicante, Ap. 99, E-03080, Alicante, Spain
[3]Dept. de Óptica, Farmacología y Anatomía, Univ. de Alicante, Ap. 99, E-03080, Alicante, Spain

ABSTRACT

We introduce a polyvinil alcohol/acrylamide (PVA/AA) photopolymer compound in a holographic memory testing platform to provide experimental results for storage and retrieval of information. We also investigate different codification schemes for the data pages addressed onto the parallel-addressed liquid crystal on silicon (PA-LCoS) device, used as the data pager, such as binary intensity modulation (BIM), and hybrid-ternary modulation (HTM), and we will see that an actual approximation for HTM can be obtained with a PA-LCoS device. We will also evaluate the effect of the time fluctuations in the PA-LCoS microdisplays onto the BIM and HTM regimes. Good results in terms of signal-to-noise ratio and bit-error ratio are provided with the experimental system and using the PVA/AA photopolymer produced in our lab, thus showing its potential and interest for future research focused on this material with highly tunable properties.

Keywords: Holographic and volume memories, liquid crystal on silicon displays, photopolymers, parallel aligned, spatial light modulation.

1. INTRODUCTION

Promise of high density recording offered by holographic data storage systems (HDSS) has attracted much attention of research groups and companies along the years[1][2]. In a holographic data storage system (HDSS), the entry data point and the recording material are the two key elements. As an entry data point spatial light modulators (SLM) enable changing the data dynamically. Parallel aligned liquid crystal on silicon microdisplays (PA-LCoS) have been widely used as SLMs. They offer an easy operation as phase-only devices and enable amplitude mostly modulation regime as well. These features bring us the opportunity to select the modulation regime required for a wide range of applications. Thus, PA-LCoS microdisplays are widely used in diffractive optics[3], optical metrology[4], reconfigurable interconnects[5][6], quantum optical computing[7] and other Optics and Photonics applications, due to their very high spatial resolution and very high light efficiency[8][9]. For all of these reasons we introduce this novel device as the SLM in our HDSS platform[10]. A major goal is to evaluate and optimize our in-house produced polyvinil alcohol/acrylamide (PVA/AA) photopolymer[11], since further efforts are still necessary to optimize this material for holographic memories, typically for write-once read-many (WORM) applications. This is a holographic recording material combining good optical properties, ease of fabrication, self-development capability and it enables producing thick recording layers, useful for multiplexing in holographic memories[12][13].

PA-LCoS displays can be assimilated to linear variable retarders but they exhibit some flicker or fluctuations[14][15], specially the digitally addressed backplane devices[16][17], widely used in most of the applications. Then, for a full characterization of the PA-LCoS device, both the retardance and the fluctuation amplitude are necessary. To this goal we demonstrated a detailed characterization technique based on time-average Stokes polarimetry[18][19]. Based on this characterization we demonstrated some benefits and limitations of applying binary intensity modulation (BIM) and hybrid-ternary modulation (HTM) with PA-LCoS devices in HDSS[10]. We verified the good performance of PA-LCoS to display BIM data pages, and we also observed that pure HTM data pages cannot be implemented, however, a rather close performance is obtained when implementing a pseudo-HTM scheme[10]. In a previous work[20] we analyzed how

Optics and Photonics for Information Processing X, edited by Khan M. Iftekharuddin, Abdul A. S. Awwal, Mireya García Vázquez, Andrés Márquez, Mohammad A. Matin, Proc. of SPIE Vol. 9970, 997008 · © 2016 SPIE · CCC code: 0277-786X/16/$18 · doi: 10.1117/12.2236113

these modulation schemes affect to the DC-term so that we can anticipate problems related with the material saturation. Now we want to make a study of the complete process, this means from modulation to data registration and finally the data page reconstruction. Thus, further details in this line of research will be given in the present work when recording data pages in a PVA-AA photopolymer layer.

2. MODULATION SCHEMES

In order to use a PA-LCoS device for HDSS some binary or multinary modulation scheme has to be selected. PA-LCoS devices are well adapted to display phase-only elements since they enable phase-only modulation of the object beam without coupled amplitude. To use the PA-LCoS as a data pager we have to define how to implement different modulation schemes. This can be achieved by illuminating the device with linearly polarized, depending on the orientation between the polarizer and the director axis we can achieve different modulation schemes. In previous works[10][20] we showed how to implement the widely used binary intensity modulation (BIM) and an approximation to hybrid ternary modulation (HTM) that we called pseudo-HTM (p-HTM). For this purpose we need to know the linear retardance and the flicker introduced by the device as a function of gray level. This relation are obtained by means of an average stokes polarimetric method developed by our group[18][19]. In this section, we investigate how to apply PA-LCoS devices to display the widely applied BIM data pages and HTM data pages. Specifically, HTM modulation scheme is very much demanding on the phase and amplitude modulation properties of the device used as SLM, thus the need to evaluate novel PA-LCoS.

2.1 Complex amplitude calculation for the PA-LCoS

To select an appropriate modulation scheme we need to analyze the phase shift and modulation capabilities of the PA-LCoS devices. Since phase-shift information is involved we use the Jones matrix formalism to calculate the complex amplitude of the light at the device exit. In order to control the electric field at the exit we inserted the LCoS device between two rotated polarizers. With this setup in mind, we calculate the electric field at the exit following equation (1):

$$\vec{E}_{OUT} = P_X \cdot R(\theta_2) \cdot W_{PA}(\Gamma) \cdot \begin{pmatrix} \cos\theta_1 \\ \sin\theta_1 \end{pmatrix} \tag{1}$$

where θ_1 and θ_2 are the angles of the linear polarizers at the system entry and exit respectively, with respect to the X-axis. The expression $W_{PA}(\Gamma)$ is the matrix for the PA-LCoS device, as the device can be considered a variable linear retarder. We provide a more detailed explanation for equation (1) in previous works[10][20]. The relation between retardance Γ and the gray level addressed in the PA-LCoS is measured with the average Stokes polarimetric technique[18].

The specific PA-LCoS device considered in this work is a commercially available PA-LCoS microdisplay, model PLUTO distributed by the company HOLOEYE. It is filled with a nematic liquid crystal, with 1920x1080 pixels and 0.7" diagonal. The pixel pitch is of 8.0 μm and the display has a fill factor of 87%. The signal is addressed via a standard DVI (Digital Visual Interface) signal. By means of the RS-232 interface and its corresponding provided software, we have access to the basic electrical parameters of the device[14], such as the digital addressing sequence format, the gamma curve, and the voltage dynamic range of the pulse width modulated (PWM) signal (through two digital potentiometers), i.e. the so-called voltages V_{bright} and V_{dark}. These V_{bright} and V_{dark} voltages express the maximum and minimum amplitudes of the pulsed voltage applied across the LC layer. In particular the software for the SLM is provided with a series of configuration files corresponding to two different digital addressing sequences: the so-called 18-6 and 5-5 digital sequences. The first number indicates the quantity of "equally weighted" bit-planes, and the second number the quantity of "binary" bit-planes[14]. This means that the sequence 18-6 is longer than the one corresponding for the sequence 5-5. In principle the shorter the sequence the smaller the flicker[14] thus in the following we restrict our attention to sequence 5-5 since it produces less flicker.

To obtain the relation of the retardance as a function of gray level we have to select a specific setup in the lab. For configuring the LCoS device the main characteristic that we have to take into account is the incidence angle between the laser beam and the LCoS screen. We have selected a 11.5º incidence angle because this will be the angle used in the HDSS setup showed in the next section. Taking into account this incidence angle we can obtain the average retardance,

$\overline{\Gamma}$, and the flicker amplitude, a, as a function of gray level using the average Stokes polarimetric technique[18]. Figure 1 shows the resultant data for the configuration selected for BIM (continuous line) and for HTM (dashed line). It is important to notice that for BIM we have reduced the average retardance range to about 180º range, whereas for HTM it is necessary a 360º range. This variation in range is performed by changing V_{bright} and V_{dark}[17]. In Fig. 1 we see that the reduction of the difference between V_{bright} and V_{dark} (see data in the caption of figure) produces a reduction in the flicker amplitude, a: for BIM the maximum fluctuation amplitude is about 15º whereas for HTM, using the full range of V_{bright} and V_{dark}, increases to a maximum of about 40º.

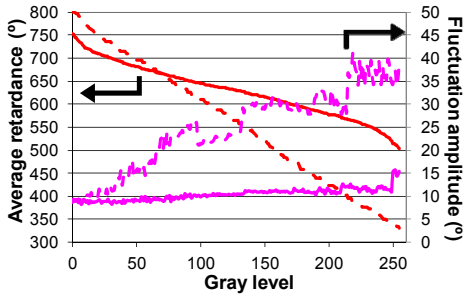

Fig. 1. Calculated values for the average retardance and the fluctuation amplitude for λ=532nm, at an angle of incidence of 11.5º, for sequence 5-5 with configuration voltages (Vbright = 2.02V, Vdark = 1.11V) for BIM (continuous) and (Vbright = 3.82V, Vdark = 0.03V) for HTM (dashed).

2.2 Binary Intensity Modulation

A BIM scheme consists in two intensity levels that define the ON and OFF values. For obtaining the best raw BER (Bit Error Rate) possible, we want to separate these intensity levels as much as possible. If we define contrast as $I_{contrast} = I_{ON} / I_{OFF}$, with a contrast of 1:20 we can obtain an acceptable raw BER (Bit Error Rate)[21]. The maximun contrast can be obtained just by using linear polarizers oriented at 45º angle with respect to the director axis of our PA-LCoS.

Combining the values measured in Fig. 1 and equation (1) we calculate the intensity transmitted and the phase-shift as a function of gray level, represented respectively in Fig. 2(a) and (b). For a deeper insight, we also include in Fig. 2(c) the phasor representation in the complex plane. We have plotted in the three figures the results when considering the values in Fig. 1 for the average retardance when adding the flicker amplitude, $\overline{\Gamma} + a$, when substracting, $\overline{\Gamma} - a$, and with no flicker, $\overline{\Gamma}$, labelled respectively as "PosFluct", "NegFluct" and "NoFluct". These figures complement results already presented[10][20] enabling an estimation for the range of the time fluctuation at each gray level (voltage value) in the intensity transmission and in the phase-shift produced by the flicker. The time fluctuation in the normalized intensity will produce a reduced intensity contrast when compared with the situation with no fluctuations. The time fluctuation in the phase-shift does not have an effect since in the BIM we only use the intensity. In Fig. 2(c) we see that the trajectory in the complex plane is almost circular. The trajectories for the three flicker amplitude cases basically overlap: their amplitude and angle at each gray level are not equal but very close since variations in Fig. 2(a) and (b) are not very big.

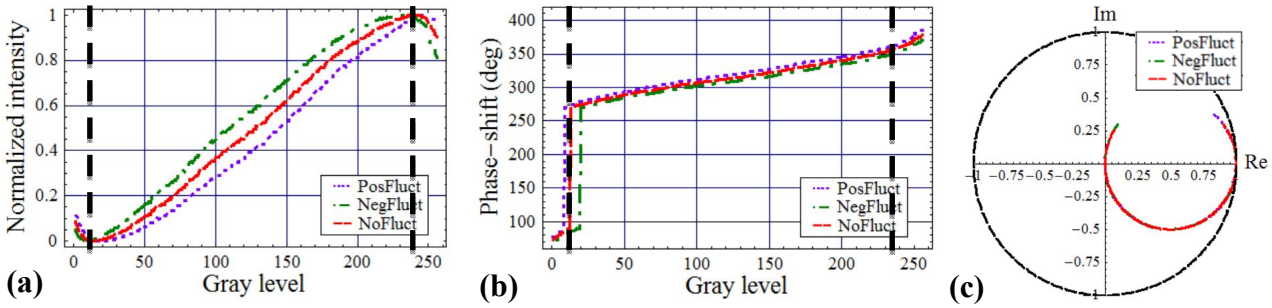

Fig. 2. Simulation for BIM. (a) Intensity transmission; (b) Phase-shift; (c) Phasor evolution in the complex plane. Only polarizers at +45º with respect to the X-axis (neutral line).

To select the appropriate gray levels that encode the ON and OFF state we consider Fig. 2(a) and the curve "NoFluct" since it is in between the two extreme situations given by "PosFluct"and "NegFluct". We select gray level 12 as OFF state, and gray level 239 as ON state, maximizing the contrast according to the calculations with the curve "NoFluct". In the experimental measurements we obtain that the low and high transmission points occur slightly displaced at gray levels 14 and 248, and the contrast we measure is about 1:50.

2.3 Hybrid Ternary Modulation

The main advantage of Hybrid-Ternary Modulation (HTM) is that it is possible to minimize the DC-term[22] while maintaining the straightforward direct intensity detection scheme used in BIM. HTM has been demonstrated and analysed with twisted-nematic LCDs[23]. We want to show in this section the problems and possible solutions when PA-LCoS devices are used to implement a HTM scheme. For implementing HTM we need three gray level values, two of them with a high and equal transmission level, and with a 180º relative phase-shift (these will be the ON levels), and a low intensity transmission level (OFF level). After performing a series of optimizations and simulations we found[10] that regardless on the orientation of the polarizers transmission axes (and neutral axes from additional external waveplates) the PA-LCoS devices cannot accomplish these requirements: since a circular trajectory is always produced in the complex plane (as the one shown in Fig. 2(c)), then the 180º phase change is produced at the origin where there is no energy transmitted. However, an approximate trade off, the pseudo-HTM (pHTM) can still be found[10] which will be next described. In the case of twisted-nematic LCDs (TN-LCDs) amplitude modulation and phase-shift are coupled, which enabled to produce spiral and other arbitrary complex amplitude trajectories in the complex plane representation[24][25].

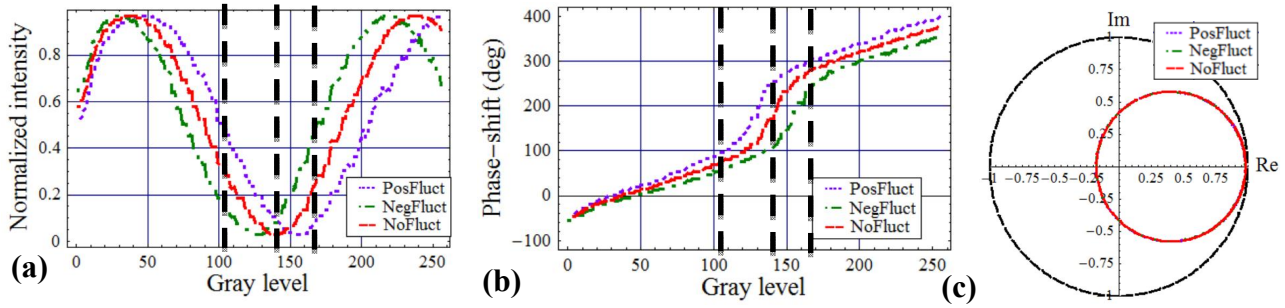

Fig. 3. Simulation for pHTM. (a) Intensity transmission; (b) Phase-shift; (c) Phasor evolution in the complex plane. Input and output polarizers at +55º and -45º with respect to the X-axis.

In Fig. 3 we show the calculated results for one of the possible pHTM configuration. These curves are obtained as in the case of BIM from the measured data in Fig. 1 (using the configuration for a full 2π phase range) and the equation (1). In this case the input polarizer is rotated 55º with respect the X-axis and the output polarizer is at -45º. We provide results, as in Fig. 2, for the three flicker amplitude cases. In Fig. 3(c) we notice that the trajectory does not cross the origin in the complex plane, so the OFF level will produce some light leakage. We shift the circular trajectory in the complex plane by changing the orientation of the input polarizer slightly from 45º, and then we obtain an approximate HTM scheme, the pHTM, with some light leakage but still a compromise close enough to the ideal HTM. The two ON gray levels considered are 105 and 168, with amplitude transmission values of 0.28 and phase-shift values of 75º and 281º respectively, i.e. a phase-shift difference of 206º. The OFF gray level is 140 with an amplitude transmission of 0.03 and phase-shift 170º. So the intensity contrast is 1:10. To extract the gray levels and the intensity transmission and phase-shift values we consider the curve "NoFluct" and plots in Fig. 3(a) and 3(b). Then, in these figures the curves for "PosFluct" and "NegFluct" tell us that the time variations will affect both the intensity contrast and the relative phase-shift values since they are fluctuating with time, which are novel results not previously shown.

Other pHTM configuration are possible. However, through simulations and in the lab[20] we have seen that to reduce the DC-Term we need to select the ON levels as close to the origin as possible, so that the relative phase-shift is not much

larger than 180º since this have a strong negative effect on the magnitude of the DC-term. Thus a better contrast ratio is possible but with no real benefits.

3. EXPERIMENTAL RESULTS

3.1 Experimental Setup

In previous section we have defined the modulation scheme that will be used for testing our HDSS. In this paper we show how accurate can be the reconstruction process and how we can calculate the raw BER for the different modulation schemes presented previously and with the PVA/AA photopolymer developed in our lab.

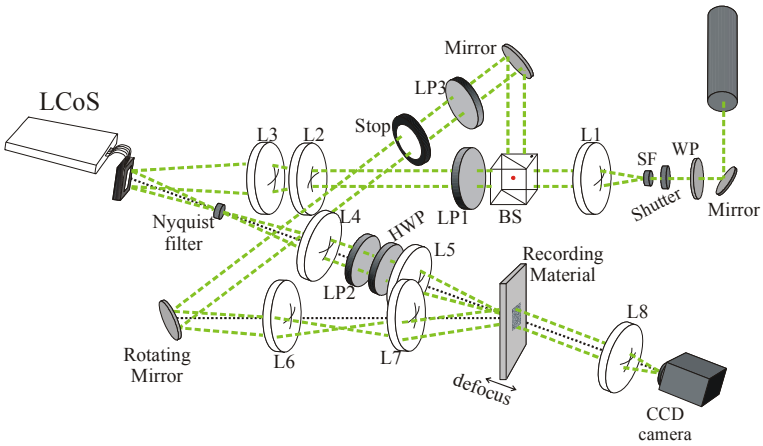

Fig. 4. Diagram for the experimental HDSS testing platform. System described in the text.

In Fig. 4 we show the scheme for the experimental holographic memory setup used in our lab. We consider the 532 nm beam from a Nd:YVO_4 laser, to which the PVA/AA photopolymer is sensitized. The main structure of the system with the object and reference arms can be clearly appreciated in the diagram. This setup has been already described with a large detail in previous works[10]. In our setup we use a convergent correlator design for the object arm, proved useful for HDSS[10]. The system enables angular multiplexing, Nyquist filtering and defocus registration onto the recording material. Furthermore, the system composed of the PA-LCoS and the input and output linear polarizers enables to generate the BIM and pHTM regimes established in previous section. In the present study we do not use the multiplexing or defocus capabilities, but we wanted to reflect the real and complete setup used in our lab.

In the reconstruction step, the recording material is illuminated with the reference beam and the lens L8 produces the Fourier transform of the object beam retrieved onto the plane of the CCD camera (pco.1600 model from pco.imaging). This is a high dynamic 14 bits cooled CCD camera system with a resolution of 1600x1200 pixels, and a pixel size of 7.4x7.4 μm^2. The magnification of the PA-LCoS plane onto the camera plane is about a factor x2.

Apart from the time flicker already described, LCoS devices exhibit other degradation effects when images with non-uniform spatial bandwidth content are addressed, such as cross-talk effects between pixels, inducing anamorphic and frequency-dependent effects[26]. To limit these effects we have preferred to work with bigger bit sizes in the image, smaller spatial frequency content. In this paper, we consider data pages on the PA-LCoS with 8x8 LCoS-pixels per bit. The size of the data pages is with 64x64 bits. We will show also show that when using a 4x4 pixel per bit size the data page retrieved worsens due to the cross-talk limitations.

3.2 Bit Error Rate calculation

We have analyzed the raw Bit Error Rate (BER) of some recorded images. For its calculation, we have applied a simple method consisting in defining a threshold level. This threshold level defines the gray level separating the "1" level bits (ON pixels) and the "0" level bits (OFF pixels), which happen below this level. We have analyzed the influence of the

position of this threshold level in the number of errors and we select the optimum threshold as the gray level reducing the the number of errors detected.

In the first place, we want to compare the different pixel size used in the PA-LCoS, for that reason we present the reconstructed image captured by the CCD without using recording material. This shows us the capacity of reconstruction of our optical system by isolating it from effects due to the recording material. As we have seen in section 2, the BIM scheme presents a better contrast ratio than the pHTM that will be reflected in a better reconstruction. For that reason we choose this scheme to test the limits of our optical setup by addressing different pixel-size per bit images in the LCoS device.

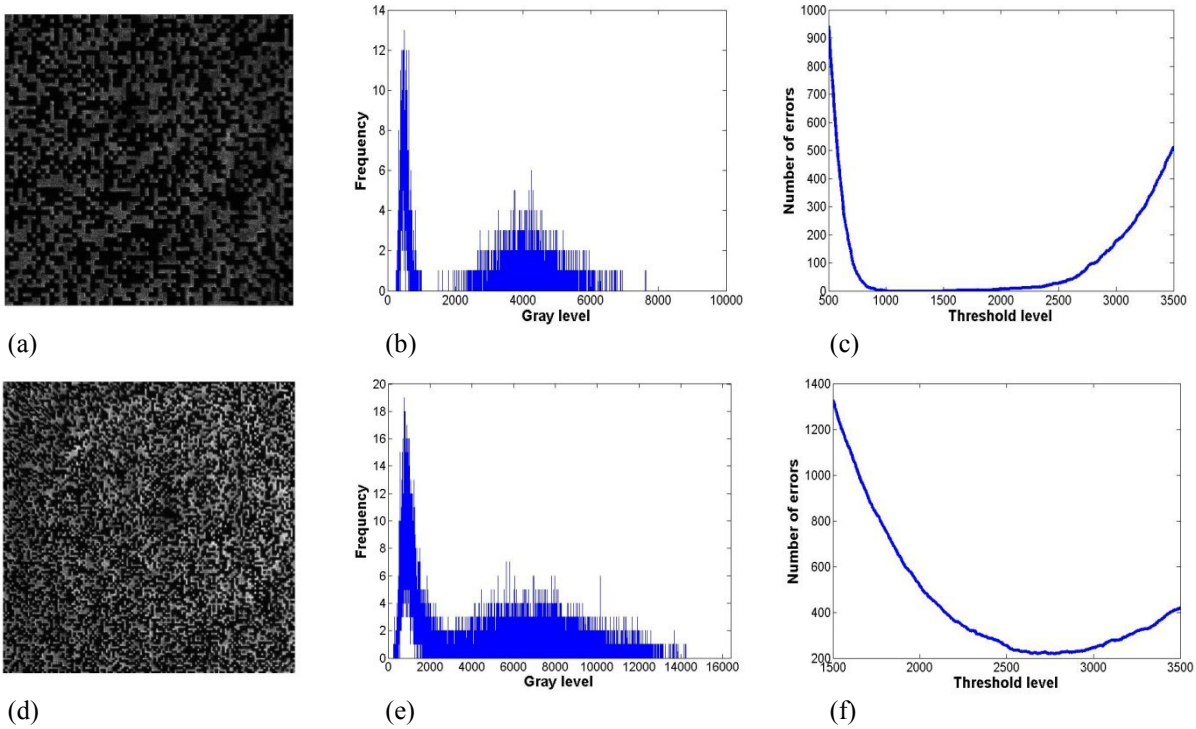

Fig. 5. (a) For 8x8 pixels per bit, image captured by the CCD, and its corresponding (b) histogram and (c) number of errors vs. threshold level. (d) For 4x4 pixels per bit, image captured by the CCD, and its corresponding (b) histogram and (c) number of errors vs. threshold level.

In Fig. 5 we show the image captured by the CCD camera for a data page with a bit size of 8x8 LCoS-pixel per bit (Fig. 5 (a)) and for a data page with bit size of 4x4 LCoS-pixel per bit (Fig. 5(d)). These first results are the reconstructed image without using recording material, the purpose of which is to evaluate the optical setup. As we can see in Fig. 5 (b), the histogram for a data page with a pixel size of 8x8 LCoS pixels is clearly divided between low levels (0's) and high levels (1's). This will allow us to reconstruct perfectly, without errors, as can be seen in Fig. 5(c). In Fig. 5(e) the histogram is not clearly divided between 0's and 1's, so it will be impossible to reconstruct without errors. From Fig. 5(f) we extract the information with about 220 errors.

From the graphics presented in Fig. 5(c) and 5(f) we can calculate the BER for the image, and from the associated histograms we can inferred how good this BER will be. There is a way to estimate the quality of the signal-to-noise ratio tipically used in digital systems, the so-called Q-factor[10], which is given by[10]:

$$Q = \frac{|\mu_1 - \mu_0|}{\sigma_1 + \sigma_0} \tag{2}$$

, where μ_1 and μ_0 are the mean value in the histograms produced for the gray level distribution of ON and OFF bits respectively, and where σ_1 and σ_0 are the corresponding standard deviations. We need BER below 10^{-2}-10^{-3} for further reduction to practical levels when error correction codes are applied. This is associated with a Q-factor value above 1.6.

The Q-factor calculated for pixel size 8x8 image in Figs. 5(a)(b)(c) is 3.81, and for the pixel size 4x4 in Figs. 5(d)(e)(f) is 2.17. In the first image the BER is zero because no errors are committed during the reconstruction, for the second image we calculate a BER of $1.3\text{x}10^{-2}$. The two images are well reconstructed but from now on, and to clearly discriminate the effect of introducing the recording material, we will present results for 8x8 pixels size. Thus, we will work with 64x64 bits data pages with a bit size of 8x8 LCoS pixels per bit.

Now we want to compare the reconstruction quality for the different modulation schemes and with the PVA/AA photopolymer. The PVA/AA photopolymer composition we use in the HDSS is similar to the one used in previous works[11]. This photo-chemical composition is characterized by the presence of yellowish eosin (YE) as dye and N,N'-methylene-bis-acrylamide (BMA) as crosslinking monomer. It also contains a co-sensitizer which is triethanolamine (TEA), the acrylamide (AA) monomer and the PVA as a binder. The thickness of the samples is around 90±2μm and the refractive index modulation achieved for a single holographic grating with a spatial frequency of 1150 lines/mm is 0.005. Thicker samples can be prepared with PVA/AA photopolymer, which is necessary when multiplexing many data pages.

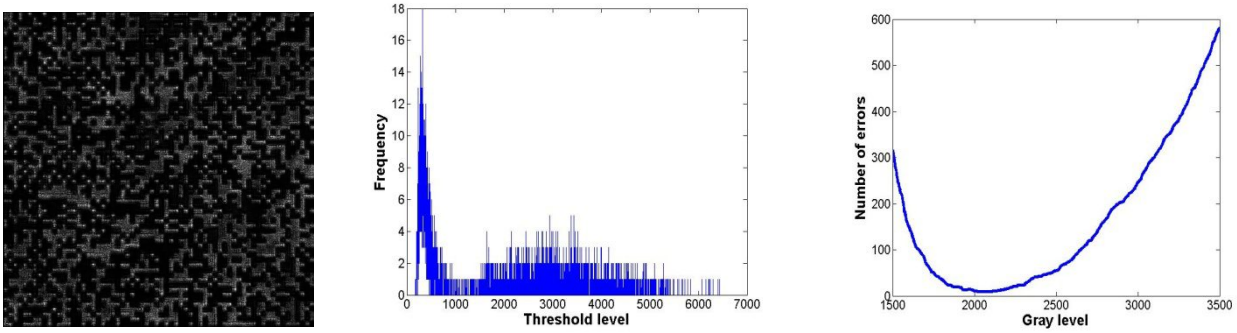

(a) (b) (c)

Fig. 6. (a) Image captured by the CCD (b) Histogram (c) Number of errors vs. threshold level. For a BIM page recorded onto the PVA/AA photopolymer and a power beam object/reference relation of 1:800.

In Fig. 6 we show an example of an image captured after reconstruction for the BIM scheme. We see that it is a good image and in the histogram represented in Fig. 6(b) it can be inferred the best level for reducing the number of errors. Figure 6(c) is a computed calculation of the number of errors vs. the threshold level from the experimentally obtained histogram. We see that this curve shows us information about how successful the reconstruction process will be. If this curve is smooth it means that the threshold level is not very demanding and we have a wider tolerance to establish it with a good reconstruction result. In the present case we can also infer this from the histogram, but sometimes it is not so clear. For this reason we use the Q-factor presented above. In this case the number of errors is 9, thus the BER is $2.0\text{x}10^{-3}$. And the value for the Q-factor calculated from the histograms is 2.52.

Now in Fig. 7 we will see the reconstructed image for the pHTM scheme and we will analyze the BER and the various magnitudes of interest.

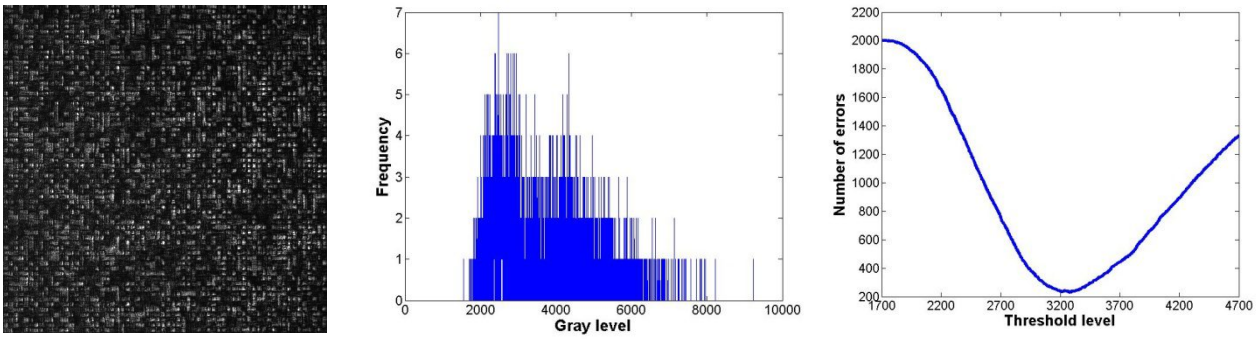

(a) (b) (c)

Fig. 7. (a) Image captured by the CCD (b) Histogram (c) Number of errors vs. threshold level. For a pHTM page recorded onto the PVA/AA photopolymer and a power beam object/reference relation of 1:800.

We show in Fig. 7(a) the captured image, and in Fig. 7(b) and (c) respectively the associated histogram and the number of errors vs. threshold level. We notice that the histogram is not useful to define the appropriate level, whereas the curve of number of errors as a function of threshold level allows us to select this threshold level. The narrower shape shows us that compared with Fig. 6 the threshold level is more critical to define the best value for reconstructing the data page. In this case the Q-factor calculated from the histogram is 1.44 and the BER calculated, 229 errors found, is $5.6x10^{-2}$.

To see if the reconstruction process will be possible, apart from the beam power relation or the exposure time, there are other aspects related with the material properties that affect the reconstructed image quality. One of the most annoying is the non-uniformity of the photopolymer. In some samples we found bubbles or ripples that deform the reconstructed image increasing the BER. In these cases the BER is increased due to the scattering effects. We are depositing the polymer by gravity in a glass substrate, during the drying process some part of the polymer can crystallize and sometimes, simply due to the depositing method, micro-bubbles appear. All these effects, and some others such as optical aberrations due to residual misalignments in the optical setup need to be carefully controlled so that the BER is kept under the required levels.

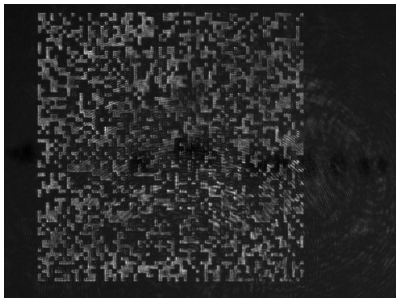

Fig. 8. Image captured in the CCD showing scattering artifacts formed due to imperfection in the photopolymer

4. CONCLUSIONS

We have presented a method to evaluate the reconstruction fidelity and the BER obtained from different recorded images. We have compared two different modulation schemes, BIM and the so-called pHTM. We see that the two of them present adequate BER results. We have presented and stressed the usefulness of the Q-factor that allows us to estimate the reconstruction fidelity from the calculated histogram, complementing the information provided by the BER. We have also provided further results to discuss the degradation effects of the time fluctuations of the PA-LCoS on the BIM and pHTM regimes. As a whole we have shown good results with the PVA/AA photopolymer produced in our lab, thus showing its potential and interest for future research focused on this material with highly tunable properties.

ACKNOWLEDGEMENTS

This work was supported by the Ministerio de Trabajo y Competitividad of Spain under projects FIS2014-56100-C2-1-P and FIS2015-66570-P and by the Generalitat Valenciana of Spain (under projects PROMETEOII/2015/015 and ISIC/2012/013) and by the University of Alicante (GRE12-14).

REFERENCES

[1] H. J. Coufal, D. Psaltis, and B. T. Sincerbox, eds., [Holographic Data Storage], Springer-Verlag (2000).
[2] K. Curtis, L. Dhar, A. Hill, W. Wilson and M. Ayres, eds., [Holographic Data Storage: From Theory to Practical Systems], John Wiley & Sons Ltd. (2010).

[3] J. Turunen and F. Wyrowski, eds., [Diffractive Optics for Industrial and Commercial Applications], Akademie Verlag (1997).
[4] W. Osten, C. Kohler, and J. Liesener, "Evaluation and application of spatial light modulators for optical metrology," Opt. Pura Apl. **38**, 71-81 (2005).
[5] M. A. F. Roelens, S. Frisken, J. A. Bolger, D. Abakoumov, G. Baxter, S. Poole, and B. J. Eggleton, "Dispersion trimming in a reconfigurable wavelength selective switch," J. Lightw. Technol. 26, 73–78 (2008).
[6] M. Salsi, C. Koebele, D. Sperti, P. Tran, H. Mardoyan, P. Brindel, S. Bigo, A. Boutin, F. Verluise, P. Sillard, M. Bigot-Astruc, L. Provost, and G. Charlet, "Mode-Division Multiplexing of 2 100 Gb/s Channels Using an LCOS-Based Spatial Modulator," J. Lightw. Technol. 30, 618–623 (2012).
[7] M. A. Solís-Prosser, A. Arias, J. J. M. Varga, L. Rebón, S. Ledesma, C. Iemmi, and L. Neves, "Preparing arbitrary pure states of spatial qudits with a single phase-only spatial light modulator," Opt. Lett. 38, 4762-4765 (2013).
[8] S. T. Wu and D. K. Yang, [Reflective Liquid Crystal Displays], John Wiley & Sons Inc. (2005).
[9] N. Collings, T. Davey, J. Christmas, D. Chu, and B. Crossland, "The Applications and Technology of Phase-Only Liquid Crystal on Silicon Devices," J. Display Technol. 7, 112-119 (2011).
[10] F.J. Martínez, R. Fernández, A. Márquez, S. Gallego, M. L. Álvarez, I. Pascual, and A. Beléndez. "Exploring binary and ternary modulations on a PA-LCoS device for holographic data storage in a PVA/AA photopolymer," Opt. Express 23, 20459-20479 (2015).
[11] S. Gallego, A. Márquez, S. Marini, E. Fernández, M. Ortuño, and I. Pascual, "In dark analysis of PVA/AA materials at very low spatial frequencies: phase modulation evolution and diffusion estimation," Opt. Express 17, 18279-18291 (2009).
[12] H. Sherif, I. Naydenova, S. Martin, C. McGinn, and V. Toal, "Characterisation of an acrylamide-based photopolymer for data storage utilizing holographic angular multiplexing," J. Opt. A: Pure Appl. Opt. 7, 255-260 (2005).
[13] E. Fernández, M. Ortuño, S. Gallego, R. García, A. Beléndez, and I. Pascual, "Comparison of peristrophic multiplexing and a combination of angular and preistrophic holographic multiplexing in a thick PVA/acrylamide photopolymer for data storage," Appl. Opt. 46, 5368-5372 (2007).
[14] A. Hermerschmidt, S. Osten, S. Krüger, and Thomas Blümel, "Wave front generation using a phase-only modulating liquid-crystalbased micro-display with HDTV resolution, " Proc. SPIE **6584**, 65840E (2007).
[15] A. Lizana, I. Moreno, A. Márquez, E. Also, C. Iemmi, J. Campos, and M.J. Yzuel, "Influence of the temporal fluctuations phenomena on the ECB LCoS performance," Proc. SPIE 7442, 74420G-1 (2009).
[16] G. Lazarev, A. Hermerschmidt, S. Krüger, and S. Osten, "LCOS Spatial Light Modulators: Trends and Applications," in [Optical Imaging and Metrology: Advanced Technologies], W. Osten and N. Reingand, eds., John Wiley & Sons (2012).
[17] F. J. Martínez, A. Márquez, S. Gallego, M. Ortuño, J. Francés, A. Beléndez, and I. Pascual, "Electrical dependencies of optical modulation capabilities in digitally addressed parallel aligned LCoS devices," Opt. Eng. 53, 067104 (2014).
[18] F.J. Martínez, A. Márquez, S. Gallego, J. Francés, I. Pascual, and A. Beléndez, "Retardance and flicker modeling and characterization of electro-optic linear retarders by averaged Stokes polarimetry," Opt. Lett. 39, 1011-1014 (2014).
[19] F.J. Martínez, A. Márquez, S. Gallego, M. Ortuño, J. Francés, A. Beléndez, and I. Pascual, "Averaged Stokes polarimetry applied to evaluate retardance and flicker in PA-LCoS devices," Opt. Express 22, 15064-15074 (2014).
[20] F.J. Martínez, A. Márquez, S. Gallego, S. Fenoll, M. Ortuño, J. Francés, S. Bleda and I. Pascual. "Analysis of holographic data storage using a PA-LCoS device" Proc. SPIE 9889. 988922 (2016).
[21] M. J. O'Callaghan, "Sorting through the lore of phase mask options - performance measures and practical commercial desing," Proc. SPIE 5362, 159 (2004)
[22] B. Das, J. Joseph, and K. Singh, "Material saturation in photopolymer holographic data recording and its effects on bit-error-rate and content-addressable search," Opt. Pura Apl. 42, 125-132 (2009)
[23] J. S. Jang and D. H. Shin, "Optical representation of binary data based on both intensity and phase modulation with a twisted-nematic liquid-crystal display for holographic digital data storage," Opt. Lett. 26(22), 1797-1799 (2001)

[24] A. Márquez, S. Gallego, D. Méndez, M. L. Alvarez, E. Fernández, M. Ortuño, C. Neipp, A. Beléndez, and I. Pascual, "Accurate control of a liquid-crystal display to produce a homogenized Fourier transform for holographic memories," Opt. Lett, 32(17), 2511-2513 (2007)
[25] E. Fernández, A. Márquez, S. Gallego, R. Fuentes, C. García, and I. Pascual, "Hybrid ternary modulation applied to multiplexing holograms in photopolymers for data page storage," J. Lightwave Technol. 28(5), 776-783 (2010)
[26] A. Márquez, C. Iemmi, I. Moreno, J. Campos and M. Yzuel, "Anamorphic and spatial frequency dependent phase modulation on liquid crystal displays. Optimization of the modulation diffraction efficiency," Otp. Express, 13(6), 2111-2119 (2005)